ISSN 0915-633X

NATIONAL INSTITUTE FOR FUSION SCIENCE

Consideration of Magnetic Field Fluctuation Measurements in a Torus Plasma with Heavy Ion Beam Probe

A. Shimizu, A. Fujisawa, S. Ohshima and H. Nakano

(Received - Feb. 24, 2004)

NIFS-796 Mar. 2004

TOKI, JAPAN

Consideration of Magnetic Field Fluctuation Measurements in a Torus Plasma with Heavy Ion Beam Probe

A. Shimizu, A. Fujisawa, S. Ohshima[1], H. Nakano[2]

National Institute for Fusion Science, Oroshi-cho, Toki-shi, Gifu 509-5292, Japan
[1]*Nagoya University, Fro-cho, Chikusa-ku, Nagoya 464-0814, Japan*
[2]*Graduate University for Advanced Studies, Toki-shi, Gifu 509-5292, Japan*

Abstract

The article discusses feasibility of magnetic fluctuation measurement with a heavy ion beam probe (HIBP) in an axisymmetric torus configuration. In the measurements, path integral fluctuation along the probing beam orbit should be considered as is similar to the density fluctuation measurements with HIBP. A calculation, based on an analytic formula, is performed to estimate the path integral effects for fluctuation patterns that have difference in profile, the correlation length, the radial wavelength, and the poloidal mode number. In addition, the large distance between the plasma and the detector is considered to lessen the path integral effect. As a result, it is found that local fluctuation of magnetic field can be properly detected with a heavy ion beam probe.

Keywords: Heavy Ion Beam Probe (HIBP), magnetic field fluctuation, path integral effect, torus plasma

1 Introduction

Heavy ion beam probe (HIBP) has been applied on many kinds of plasma confinement devices, such as mirror (TMX[1], GAMMA10[2]), bumpy torus (NBT[3]), reversed field pinch (MST[4]), tokamak (ISX-B[5], TEXT[6], JIPP-TIIU[7], T-10[8], JFT-2M[9]), and stellarator (ATF[10], CHS[11], LHD[12]). This is because HIBP has a unique capability to simultaneously sense potential, density and magnetic field of the interior of high temperature plasmas. In addition, the highly temporal and spatial resolution with HIBP allows us to detect the fluctuations of these physical quantities. Until now, HIBPs have been mainly used to measure density fluctuation, potential fluctuation [13], and potential profile, and the results have contributed to the clarification of phenomena associated with plasma confinement; *e.g.*, anomalous transport, barrier formation [14], bifurcation and transition [15]. However, a quite few trials have been done on the measurements with HIBP on density profile [16], magnetic field profile, and magnetic field fluctuation [17, 18], although the expected results are fascinating.

The measurement of magnetic field is very attractive, because a few diagnostics can measure the magnetic field in the plasma. In HIBP measurements, the information of magnetic field is obtained from changes of beam orbits. It is difficult to know the full orbit change due to variations of equilibrium magnetic field. On the other hand, it is easy to know the fluctuated displacement of beam at the detector. This reflects mainly the local magnetic field fluctuation, so we can measure it by HIBP. However, in this fluctuation measurement, the beam displacement is not only caused by a local fluctuation but also by a fluctuation along the beam orbit. This situation is similar to that of density fluctuation. A number of works are available on this contamination called "path integral effect" [19, 20, 21], however, there is few works for the path integral effects of magnetic field fluctuation measurements with HIBP.

In this article, a model of the path integral effect is presented after a brief description of HIBP diagnostics. For several profiles of magnetic fluctuation, difference between real fluctuation property and detected signals including the path integral contamination are calculated based on this model. In addition, the suitable geometry of an HIBP system, the position of an energy analyzer, is studied to increase accuracy of the magnetic field measurement. The feasibility of the method is discussed, with the minimum detectable fluctuation level with this method.

2 Mathematical Preparation and Calculation Model

2.1 Principle of magnetic fluctuation measurement

An HIBP system consists of beam injector or accelerator and energy analyzer, as is shown in Fig.1a. Usually, single ionized heavy ion beam (or primary beam) is injected into plasma from the beam gun, and doubly ionized ions are created through electron impact ionization in the plasma. The doubly ionized beam (or secondary beam) comes out from plasma and detected at the energy analyzer. Usually Proca and Green type analyzer [22]

is used as an energy analyzer, and the beam is detected with so-called a split plate detector (see Fig.1b). The detected beam intensity contains information of plasma density at an observation point, while the vertical and horizontal movements on the detector plates give the information of potential and magnetic field, respectively.

Supposed that the magnetic configuration be axisymmetric like tokamak, the horizontal movement can be described in an analytic form, since the canonical momentum of toroidal direction is conserved. The relation of momentum conservation along the primary orbit is written as,

$$mR^2\dot{\phi} + qRA_\phi = qR_gA_{\phi g}. \tag{1}$$

Here, m is the beam ion mass, R the major radius, ϕ the toroidal angle, dot means the time derivative, q the charge of an electron, and A_ϕ the toroidal component of vector potential. The right hand side is an initial value, and $A_{\phi g}$, R_g are the toroidal component of vector potential and major radius at the beam gun (or beam injection point) respectively. The initial velocity in the toroidal direction is assumed to be zero *i.e.* $\dot{\phi}_g = 0$, for conciseness. On the other hand, the conservation law along the secondary orbit is expressed as follows,

$$mR^2\dot{\phi} + 2qRA_\phi = qR_sA_{\phi s} + qR_gA_{\phi g}, \tag{2}$$

where R_s and $A_{\phi s}$ represent the major radius and vector potential at an observation point, respectively. After the ionization, the beam ions experience an increase in the vector potential by $qR_sA_{\phi s}$. The toroidal displacement of the beam at the detector position can be obtained by integrating these two equations. Then, the normalized toroidal displacement or toroidal angle displacement is expressed in the following form,

$$\begin{aligned}\phi_D &= \int_0^{t_d}\dot{\phi}dt = \frac{1}{v}\int_0^{\ell_d}\dot{\phi}d\ell, \\ &= \frac{qR_sA_{\phi s}}{mv}\int_{\ell_s}^{\ell_d}\frac{1}{R^2}d\ell + \frac{qR_gA_{\phi g}}{mv}\int_0^{\ell_d}\frac{1}{R^2}d\ell \\ &\quad -\frac{q}{mv}\int_0^{\ell_s}\frac{A_\phi}{R}d\ell - \frac{2q}{mv}\int_{\ell_s}^{\ell_d}\frac{A_\phi}{R}d\ell.\end{aligned} \tag{3}$$

Where v is the velocity of a beam ion, which is assumed to be constant, namely the effect of plasma potential is neglected, and t_d is the time at which a beam ion reaches to the detector position. The integral about time, t, is replaced to the integral about the path length, ℓ, in this equation. The fluctuated component of the toroidal angle of beam displacement can be written as,

$$\begin{aligned}\tilde{\phi}_D &= \frac{qR_s\tilde{A}_{\phi s}}{mv}\int_{\ell_s}^{\ell_d}\frac{1}{R^2}d\ell + \frac{qR_g\tilde{A}_{\phi g}}{mv}\int_0^{\ell_d}\frac{1}{R^2}d\ell \\ &\quad -\frac{q}{mv}\int_0^{\ell_s}\frac{\tilde{A}_\phi}{R}d\ell - \frac{2q}{mv}\int_{\ell_s}^{\ell_d}\frac{\tilde{A}_\phi}{R}d\ell.\end{aligned} \tag{4}$$

Therefore, the fluctuation of the beam movement on the detector plate can be estimated using this formula by multiplying the major radius of the detector position R_d to the toroidal angle displacement $\tilde{\phi}_D$.

2.2 Calculation Model

For the normalization and using non-dimensional variables in the calculation, Eq. (4) is transformed into the following form,

$$\begin{aligned}\tilde{\phi}_D &= \frac{R_0}{r_L}\delta_0\hat{\phi}_D, \\ \hat{\phi}_D &\equiv \hat{R}_s\tilde{\alpha}_\phi(\hat{\boldsymbol{r}}_s)\int_{\hat{\ell}_s}^{\hat{\ell}_d}\frac{1}{\hat{R}^2}\,d\hat{\ell} + \hat{R}_g\tilde{\alpha}_\phi(\hat{\boldsymbol{r}}_g)\int_0^{\hat{\ell}_d}\frac{1}{\hat{R}^2}d\hat{\ell} \\ &\quad - \int_0^{\hat{\ell}_s}\frac{\tilde{\alpha}_\phi(\hat{\boldsymbol{r}})}{\hat{R}}d\hat{\ell} - 2\int_{\hat{\ell}_s}^{\hat{\ell}_d}\frac{\tilde{\alpha}_\phi(\hat{\boldsymbol{r}})}{\hat{R}}d\hat{\ell}. \end{aligned} \tag{5}$$

Here, $r_L = mv/(qB_0)$, $\hat{R} = R/R_0$, $\hat{R}_s = R_s/R_0$, $\hat{R}_d = R_d/R_0$, $\hat{\ell} = \ell/R_0$. The parameters R_0 and B_0 are the major radius and toroidal magnetic field strength that characterize an experimental device, respectively. The function $\tilde{\alpha}_\phi$ is the normalized vector potential, of which maximum is one, with δ_0 being the maximum level of $\tilde{A}_\phi/(B_0R_0)$. Hence, $\delta_0\tilde{\alpha}_\phi \equiv \tilde{A}_\phi/(B_0R_0)$. Note that $\tilde{\alpha}_\phi$ is a function of the position vector $\hat{\boldsymbol{r}}$. $\hat{\phi}_D$ is the beam angle displacement to the toroidal direction normalized by $R_0\delta_0/r_L$. Then, the fluctuation power is written as

$$\left\langle\hat{\phi}_D^2\right\rangle = A_1 + A_2 + A_3 + B_1 + B_2 + B_3 + B_4 + C_1 + C_2 + C_3. \tag{6}$$

Here the bracket $< \cdots >$ means the ensemble average, and the symbols are

$$A_1 \equiv \left\langle\left(G_1\hat{R}_s\tilde{\alpha}_\phi(\hat{\boldsymbol{r}}_s)\right)^2\right\rangle, \tag{7}$$

$$A_2 \equiv \left\langle\left(G_2\hat{R}_g\tilde{\alpha}_\phi(\hat{\boldsymbol{r}}_g)\right)^2\right\rangle, \tag{8}$$

$$A_3 \equiv G_1G_2\hat{R}_s\hat{R}_g\left\langle\tilde{\alpha}_\phi(\hat{\boldsymbol{r}}_s)\tilde{\alpha}_\phi(\hat{\boldsymbol{r}}_g)\right\rangle, \tag{9}$$

$$B_1 \equiv -2G_1\hat{R}_s\int_{\hat{0}}^{\hat{\ell}_s}\left\langle\tilde{\alpha}_\phi(\hat{\boldsymbol{r}}_s)\tilde{\alpha}_\phi(\hat{\boldsymbol{r}}_1)\right\rangle\frac{1}{\hat{R}(\hat{\boldsymbol{r}}_1)}d\hat{\ell}_1, \tag{10}$$

$$B_2 \equiv -4G_1\hat{R}_s\int_{\hat{\ell}_s}^{\hat{\ell}_d}\left\langle\tilde{\alpha}_\phi(\hat{\boldsymbol{r}}_s)\tilde{\alpha}_\phi(\hat{\boldsymbol{r}}_2)\right\rangle\frac{1}{\hat{R}(\hat{\boldsymbol{r}}_2)}d\hat{\ell}_2, \tag{11}$$

$$B_3 \equiv -2G_2\hat{R}_g\int_{\hat{0}}^{\hat{\ell}_s}\left\langle\tilde{\alpha}_\phi(\hat{\boldsymbol{r}}_g)\tilde{\alpha}_\phi(\hat{\boldsymbol{r}}_1)\right\rangle\frac{1}{\hat{R}(\hat{\boldsymbol{r}}_1)}d\hat{\ell}_1, \tag{12}$$

$$B_4 \equiv -4G_2\hat{R}_g\int_{\hat{\ell}_s}^{\hat{\ell}_d}\left\langle\tilde{\alpha}_\phi(\hat{\boldsymbol{r}}_g)\tilde{\alpha}_\phi(\hat{\boldsymbol{r}}_2)\right\rangle\frac{1}{\hat{R}(\hat{\boldsymbol{r}}_2)}d\hat{\ell}_2, \tag{13}$$

$$C_1 \equiv \int_{\hat{0}}^{\hat{\ell}_s}\int_{\hat{0}}^{\hat{\ell}_s}\left\langle\tilde{\alpha}_\phi(\hat{\boldsymbol{r}}_1)\tilde{\alpha}_\phi(\hat{\boldsymbol{r}}_1')\right\rangle\frac{1}{\hat{R}(\hat{\boldsymbol{r}}_1)\hat{R}(\hat{\boldsymbol{r}}_1')}d\hat{\ell}_1d\hat{\ell}_1', \tag{14}$$

$$C_2 \equiv 4\int_{\hat{\ell}_s}^{\hat{\ell}_d}\int_{\hat{\ell}_s}^{\hat{\ell}_d}\left\langle\tilde{\alpha}_\phi(\hat{\boldsymbol{r}}_2)\tilde{\alpha}_\phi(\hat{\boldsymbol{r}}_2')\right\rangle\frac{1}{\hat{R}(\hat{\boldsymbol{r}}_2)\hat{R}(\hat{\boldsymbol{r}}_2')}d\hat{\ell}_2d\hat{\ell}_2', \tag{15}$$

$$C_3 \equiv 4\int_{\hat{0}}^{\hat{\ell}_s}\int_{\hat{\ell}_s}^{\hat{\ell}_d}\left\langle\tilde{\alpha}_\phi(\hat{\boldsymbol{r}}_1)\tilde{\alpha}_\phi(\hat{\boldsymbol{r}}_2)\right\rangle\frac{1}{\hat{R}(\hat{\boldsymbol{r}}_1)\hat{R}(\hat{\boldsymbol{r}}_2)}d\hat{\ell}_1d\hat{\ell}_2, \tag{16}$$

$$G_1 \equiv \int_{\hat{\ell}_s}^{\hat{\ell}_d} \frac{1}{\hat{R}(\hat{\boldsymbol{r}}_2)^2} d\hat{\ell}_2, \tag{17}$$

$$G_2 \equiv \int_0^{\hat{\ell}_d} \frac{1}{\hat{R}(\hat{\boldsymbol{r}})^2} d\hat{\ell}. \tag{18}$$

A_1 represents the local fluctuation power of magnetic field to be observed, while the other terms are contaminations; A_2 the local fluctuation power at beam gun, A_3 the correlation between two local terms, B_i the cross terms between the fluctuation on the orbits and local points, and C_i the cross terms between primary and secondary orbits. G_1 and G_2 are geometrical factors which depend on only the beam orbit.

2.3 Model of Cross Correlation Terms

In Eqs. (7-18), the path integral terms can be evaluated if the cross correlation of vector potential are given. The correlation term of $\langle \tilde{\alpha}_\phi(\hat{\boldsymbol{r}}_i)\tilde{\alpha}_\phi(\hat{\boldsymbol{r}}_j)\rangle$ is assumed as,

$$\langle \tilde{\alpha}_\phi(\hat{\boldsymbol{r}}_i)\tilde{\alpha}_\phi(\hat{\boldsymbol{r}}_j)\rangle = P(\hat{\boldsymbol{r}}_i, \hat{\boldsymbol{r}}_j)\gamma(\hat{\boldsymbol{r}}_i, \hat{\boldsymbol{r}}_j)\Psi(\hat{\boldsymbol{r}}_i, \hat{\boldsymbol{r}}_j). \tag{19}$$

Here, P is the product of amplitude of normalized fluctuation $\tilde{\alpha}_\phi(\hat{\boldsymbol{r}}_i)$ and $\tilde{\alpha}_\phi(\hat{\boldsymbol{r}}_j)$, γ and Ψ are the coherence and the difference in phase between these fluctuations. A radial profile of amplitude of $\tilde{\alpha}_\phi(\hat{\boldsymbol{r}}_i)$ is assumed to be, $\exp\left(-\left(\hat{r}-\hat{r}_0\right)^2/\hat{r}_w^2\right)$ in plasma. r is the minor radius, and r_0 is the radial position where the amplitude has maximum. r_w is the width of amplitude. The hat of these variables means the normalization by R_0. The product of fluctuation amplitude, P, is expressed as follows,

$$P = \exp\left(-\left(\hat{r}_i-\hat{r}_0\right)^2/\hat{r}_w^2\right)\cdot\exp\left(-\left(\hat{r}_j-\hat{r}_0\right)^2/\hat{r}_w^2\right). \tag{20}$$

In the outside of plasma, the radial profile of amplitude of $\tilde{\alpha}_\phi$ is assumed to be $\exp\left(-\left(\hat{a}-\hat{r}_0\right)^2/\hat{r}_w^2\right)\cdot(\hat{a}/\hat{r})^m$ as is seen in Ref. [17], where $\hat{a}$ is the minor radius of outermost magnetic surface normalized by R_0, m the poloidal mode number. The coherence γ and the difference in phase Ψ between the fluctuations are assumed as,

$$\gamma = \exp\left(-|\hat{\boldsymbol{r}}-\hat{\boldsymbol{r}}|^2/\hat{\ell}_c^2\right), \tag{21}$$

$$\Psi = \cos\left(m\left(\theta_i-\theta_j\right)\right)\cdot\cos\left(\left(\hat{r}_i-\hat{r}_j\right)/\left(2\pi\hat{\lambda}_r\right)\right). \tag{22}$$

Here, $|\boldsymbol{r}-\boldsymbol{r}|$ is the distance between two points under consideration, ℓ_c the correlation length, m the poloidal mode number, θ_i, θ_j the poloidal angles, r_i, r_j the minor radiuses, λ_r the wave length of fluctuation to the radial direction. The hat of these variables means the normalization by R_0 as described above. We will change the values of $\hat{r}_0, \hat{\ell}_c, m, \hat{\lambda}_r$ and investigate the effect of these parameters on the path integral terms in the function, $\hat{\phi}_D$.

3 Calculation Results

3.1 Path Integral Effects for Fluctuation Patterns

Here we calculate path integral effects or contaminations for three patterns of fluctuation to show possibility of the magnetic field measurement with HIBP. The assumed HIBP geometry and orbits for the calculation are shown in Fig.1a; The beam injection point $(\hat{R}_g, \hat{Z}_g)$ is (1.0, 0.7), the detection point $(\hat{R}_d, \hat{Z}_d)$ is (1.7, 0.05) respectively. The cross section of torus is circular, and the toroidal magnetic field is proportional to $1/\hat{R}$. The ratio of the major radius to the Larmor radius, R_0/ρ_L, is 2.3. Figure 2 upper shows assumed fluctuation patterns of vector potential $\tilde{\alpha}_\phi(\hat{\boldsymbol{r}})$ in the power function, $\hat{P}_i$. Here, we define $\hat{P}_i \equiv \exp\left(-\left(\hat{r}-\hat{r}_0\right)^2/\hat{r}_w^2\right)$, and consider three cases for $\hat{r}_0, \hat{r}_w$: (A) $\hat{r}_0 = 0.05, \hat{r}_w = 0.03$, the fluctuation profile has peak near center, (B) $\hat{r}_0 = 0.11, \hat{r}_w = 0.05$, peak at half radius, (C) $\hat{r}_0 = 0.17, \hat{r}_w = 0.05$, peak near the edge. In order to give a perspective, Fig.2 lower shows the calculation results of the angle displacement, $\sqrt{\left\langle \hat{\phi}_D^2 \right\rangle}$, and local term $\sqrt{A_1}$, which are shown as thick lines and thin lines respectively. The assumed parameters are $m = 2, \hat{\ell}_c = 0.1, \hat{\lambda}_r = 0.1$ in this calculation. In case (A), no significant contamination can be found both in the central and outer regime. This is because $\tilde{\alpha}_\phi \approx 0$ is valid except the central regime and path integral becomes small for the orbit to observe outer regime of plasma. However in case (C) the path integral effect is large in the central regime. The beam orbit to observe plasma center passes through the outer regime of plasma where $\tilde{\alpha}_\phi$ has a significant value.

Sensitivity of the path integral effects is examined to variation of the fluctuation parameters, correlation length, radial wavelength and poloidal mode numbers. First, the effect of correlation length $\hat{\ell}_c$ is investigated. $\hat{\ell}_c$ is changed from 0.01 to 0.2. The other parameters, $\hat{\lambda}_r, m$ are fixed to 0.1, 2 respectively. The calculated angle displacements for the profiles of fluctuation are shown in Fig.3a. The square root of local term, $\sqrt{A_1}$, is also expressed as thin solid lines. In case (A), the difference between the beam angle displacement and local term is small for any value of $\hat{\ell}_c$. In case (B) and (C), if $\hat{\ell}_c \leq 0.01$, the beam angle displacement shows good agreement with local term at the peak of fluctuation. However around the center of plasma in case (C) the beam angle displacement does not show agreement with local term.

Second, the results of scan of $\hat{\lambda}_r$ are shown in Fig.3b, which are similar to $\hat{\ell}_c$ scan. In this scan, m and $\hat{\ell}_c$ are fixed to 2 and 0.1 respectively. In case (A), the path integral effect is small, however in case (C) it becomes larger. As the radial wave length becomes smaller, the result shows that the path integral effect becomes smaller. Path integral contribution around the center is more sensitive to $\hat{\lambda}_r$ than $\hat{\ell}_c$. If $\hat{\lambda}_r \leq 0.01$, the path integral terms become small sufficiently in all cases from (A) to (C). For $\hat{\lambda}_r \leq 0.01$, the remained difference around the plasma center in case (C) is due to the effect of the local term at beam gun, A_2.

Finally, the results of m scan are shown in Fig.3c. The poloidal number m is changed from 1 to 3. In this case, $\hat{\ell}_c, \hat{\lambda}_r$ are fixed to 0.1, 0.1 respectively. In case (A), the difference

of the beam angle displacement and the local term is small, and its dependence on m is very small. However in case (C), the difference at plasma center for $m = 1$ is very large. The angle between a primary beam orbit and a secondary beam orbit is about $\pi/4$ radian in our case. When $m = 1$, this angle corresponds to only one 4th of wavelength, therefore the reduction of path integral cannot be expected. For $m = 2$, the angle corresponds to one half of wavelength, by which the reduction of path integral can be expected.

It is interesting to know which term is large in path integral terms. The profiles of these terms are shown in Fig.4. In this case, the parameters for fluctuation, $\hat{\ell}_c, \hat{\lambda}_r$ and m are set to 0.1, 0.1 and 2. The largest term in path integral terms is B_2, which is the first order path integral term on secondary beam path. Since the charge number of secondary beam is twice of that of primary beam, B_2 is twice larger than B_1. The 2nd largest term is B_1, which is the same magnitude and the opposite sign of C_2 in this case, therefore B_1 is cancelled out with C_2. The C_1, C_3 are small but cannot be ignored. Other terms are very small and can be ignored except A_2 in case (C). This term cannot be ignored only in the case (C), because the amplitude at beam gun is not small sufficiently. In the region near the plasma center, this term is dominant one of the beam angle displacement.

3.2 The effect of the diagnostic position on the magnetic fluctuation measurement

The Eq.(6) includes the geometrical factor G_1 and G_2. The squares of these factors are included in A_1 and A_2, and the factors are included in B_1, B_2, B_3 and B_4. As G_1 becomes larger, hence, the term A_1 increases more rapidly than B_1, B_2 and other terms. Thus, G_1 has an effect of magnifying the contribution of the local term A_1 to the fluctuation amplitude $\hat{\phi}_D^2$, and leads to the relative reduction of path integral effects. The factor G_1 can be enhanced by setting the diagnostic point farther away from plasma, because the length of path becomes longer. Note $\tilde{\alpha}_\phi$ becomes negligibly small in the outside of plasma, hence the integral terms including $\tilde{\alpha}_\phi$ do not contribute significantly.

In order to investigate this geometrical (or HIBP configuration) effect, the path integral effect is calculated for several cases that the major radius of diagnostics point is different. The calculation results are shown in Fig.5a and 5b. The parameters of fluctuation are, $\ell_c = 0.1, \lambda_r = 0.1, m = 2$. We consider two cases (B) and (C), because in case (A) the path integral effect is already small. In Fig.5a, the profile of beam angle displacement $\sqrt{\left\langle \hat{\phi}_D^2 \right\rangle}$, and local term $A_1^{0.5}$ are shown for the major radius of diagnostic point $\hat{R} = 1.53, 1.87, 2.38$. The magnitude of displacement is larger and the local term becomes dominant as major radius of detection point increases.

Fig.5b shows the dependence of individual path integral terms on the detector position. All terms are normalized by the square root of local term, $A_1^{0.5}$, and their absolute values are shown in the figure. The path integral contribution $\left(A_1 - \left\langle \hat{\phi}_D^2 \right\rangle\right)^{0.5} / A_1^{0.5}$ is shown as solid line. In case (B), the values of these terms at $\rho = 0.55$ are shown, where the fluctuation amplitude is maximum, and in case (C) at $\rho = 0.85$. For $\hat{R} \geq 1.7$, all terms decrease with the increase of $\hat{R}$, since G_1 becomes larger, while $B_2^{0.5}/A_1^{0.5}$ is increased

when $\hat{R}$ is changed from 1.5 to 1.7.

The geometrical factor G_1 is the integral of $1/\hat{R}^2$, therefore, for a larger value of $\hat{R}$ the improvement of path integral effect cannot be expected since rising rate of G_1 becomes slower. In fact, this tendency is seen for the region of $\hat{R} \geq 2.3$ in Fig.5b. Consequently, $\hat{R} \approx 2.3$ is the best detector position for accurate measurement of magnetic field fluctuation amplitude.

4 Discussion

So far, we have investigated feasibility of magnetic field fluctuation measurement using HIBPs by performing the calculation of beam movement for assumed three patterns of magnetic fluctuation. The findings are as follows. (1) The path integral effect is so small that the fluctuation profile can be deduced for the case that the magnetic field fluctuation is localized in the plasma core, independently of the fluctuation properties, *e.g.*, $\hat{\ell}_c, \hat{\lambda}_r, m$. (2) However, if the fluctuation is localized in an outer region of the plasma, the path integral effect becomes larger, particularly, a false signal appears in the central regime of plasma. (3) The path integral effects can be lessened if detector position is kept as far as possible from the plasma.

Magnetic field shielding effect due to vacuum vessel and others is not considered in our calculation. If this shielding effect is taken into account, the path integral contribution associated with A_2, fluctuation of vector potential at the injection point, should be smaller. Actually in the case of edge-localized fluctuation, the signal distortion in the plasma core comes mainly from this effect. In Fig.2, the false angle displacement in case (C) is reduced from 0.13 to 0.052 at the center if the term A_2 is neglected. Thus, the path integral effect is expected to be negligible for the magnetic field fluctuation localized in an outer region.

In HIBP measurements, so-called a split plate detector is used to measure the beam movement in the energy analyzer. A schematic view of the detector is shown in Fig. 1b. In this detector, the horizontal beam displacement, d, can be expressed as $d = (\Delta w/2)(i_R - i_L)/(i_R + i_L)$, where i_R and i_L are the beam currents on the right and left plates, and Δw is the horizontal beam width. In this method, the beam movement of $\sim 50\mu$m can be detected, with assumption of $(i_R + i_L) = 100$nA, $\Delta w = 5$ mm, and the minimum detectable current of 1nA.

From the formula to describe the beam displacement $d_{\min} = \sqrt{\left\langle \hat{\phi}_D^2 \right\rangle} \times \frac{R_0}{r_L} \delta_{0,\min} R_d$, the minimum detectable fluctuation $\delta_{0,\min}$ is 2.6×10^{-5} for the case of $R_0 = 1$ m, $r_L \approx 0.44$ m, $R_d = 1.7$ m, $\sqrt{\left\langle \hat{\phi}_D^2 \right\rangle} \approx 0.5$. This assumption corresponds to the case that 70keV cesium beam for magnetic field strength $B_t = 1$ T. Therefore, quite high sensitivity can be attained in magnetic field fluctuation measurement with HIBPs.

Finally, it is worth a while to touch a real trial of this method that has been ever performed. In the TEXT tokamak, a magnetic field fluctuation profile was measured actually with 500keV HIBP system using Thallium beam [18]. This magnetic field fluctuation was distributed around $\rho \sim 0.5$, with the maximum amplitude of $\delta A/(B_0 R_0) \sim 10^{-3}$

fluctuation. In the experiments, the minimum detectable resolution was seemingly 10^{-4}. The fluctuation profile is very similar to the case (B) in this article. According to our calculation result, the path integral effect is sufficiently small to deduce the real fluctuation pattern.

In conclusion, we have considered the path integral effects in magnetic field fluctuation measurement with HIBP. Our consideration shows that the path integral effect can be negligible for a wide variety of fluctuation patterns, if the HIBP geometry is appropriately chosen; it is better if the beam injection and detection points are located at a sufficient distance from the plasma. This method should be quite promising since the method provides a high sensitivity of magnetic fluctuation, less than 10^{-4}, with high resolutions of space ($\sim$ mm) and time ($\sim \mu$s).

Acknowledgments

The authors thank H. Iguchi, K. Matsuoka, S. Okamura and other members of CHS-group for their continuous supports.

References

[1] G. A. Hallock, R. L. Hickok, R. S. Hornady, IEEE Trans. Plasma Sci. **22**, 341 (1994).

[2] K. Isii, IEEE Trans. Plasma Sci. **22**, 332 (1994).

[3] K. Takasugi, H. Iguchi, M. Fujiwara, H. Ikegami, Japanese Journal of Appl. Phys. **23**, 364 (1984).

[4] U. Shah, K. A. Connor, J. Lei, P. M. Schoch, T. P. Crowley, J. G. Schatz, Y. Dong, Rev. Sci. Instrum. **70**, 963 (1999).

[5] G. A. Hallock, A. J. Wootton, R. L. Hickok, Phys. Rev. Lett. **59**, 1301 (1987).

[6] J. C. Forster, P. M. Schoch, R. L. Hickok, W. C. Jennings, IEEE. Trans. Plasma Sci. **22**, 359 (1994).

[7] Y. Hamada, A. Nishizawa, Y. Kawasumi, A. Fujisawa, H. Iguchi, Fus. Eng. Des. **34-35**, 663 (1997).

[8] A. Melnikov, L. Eliseev, K. Razumova, I. Bondarenko, L. Krupnik, S. Khrebtov, A. Komarov, A. Kozachek, J. Plasma Fusion Res. SERIES **3**, 46 (2000).

[9] T. Ido, Y. Hamada, A. Nishizawa, Y. Kawasumi, Y. Miura, K. Kamiya, Rev. Sci. Instrum. **70**, 955 (1999).

[10] K. A. Connor, J. J. Zielinski, J. G. Schwelberger, S. C. Aceto, Rev. Sci. Instrum. **63**, 4505 (1992).

[11] A. Fujisawa, H. Iguchi, S. Lee, T. P. Crowley, Y. Hamada, S. Kubo, H. Idei, H. Sanuki, K. Itoh *et. al.*, Phys. Plasmas **4** 1357 (1997).

[12] A. Taniike, M. Sasao, A. Fujisawa, H. Iguchi, Y. Hamada, J. Fujita, M. Wada, Y. Mori, IEEE Trans. Plasma Sci. **22**, 430 (1994).

[13] G. A. Hallock, P. M. Schoch, K. Saadatmand, R. L. Hickok, W. C. Jennings, K. A. Connor, Rev. Sci. Instrum. **56**, 1038 (1985).

[14] T. Ido, K. Kamiya, Y. Miura, Y. Hamada, A. Nishizawa, Y. Kawasumi, Phys. Rev. Lett. **88**, 055006 (2002).

[15] A. Fujisawa, H. Iguchi, T. Minami, Y. Yoshimura, H. Sanuki, K. Itoh, M. Isobe, S. Nishimura, C. Suzuki, K. Tanaka, M. Osakabe, I. Nomura, K. Ida, S. Okamura, K. Toi *et. al.*, Nucl. Fusion **41**, 575 (2001).

[16] A. Fujisawa, M. Kitazawa, A. Shimizu, S. Ohshima, H. Iguchi, Rev. Sci. Instrum. **74**, 3335 (2003).

[17] V. J. Simicic, K. A. Connor, T. P. Crowley, R. L. Hickok, P. M. Schoch, A. J. Wootton, X. Z. Yang, Y. Z. Zhang, Rev. Sci. Instrum. **61**, 3061 (1990).

[18] V. J. Simcic, T. P. Crowley, P. M. Schoch, A. Y. Aydemir, X. Z. Yang, K. A. Connor, R. L. Hickok, A. J. Wootton, S. C. McCool, Phys. Fluids **B 5**, 1576 (1993).

[19] D. W. Ross, M. L. Sloan, A. J. Wootton, P. M. Schoch, J. W. Heard, T. P. Crowley, R. L. Hickok, V. Simcic, Rev. Sci. Instrum. **63**, 2232 (1992).

[20] J. W. Heard, T. P. Crowley, D. W. Ross, P. M. Schoch, R. L. Hickok, Jr., B. Z. Zhang, Rev. Sci. Instrum. **64**, 1001 (1993).

[21] A. Fujisawa, H. Iguchi, S. Lee, Y. Hamada, Rev. Sci. Instrum. **68**, 3393 (1997).

[22] G. A. Proca, T. S. Green, Rev. Sci. Instrum. **41**, 1778 (1970).

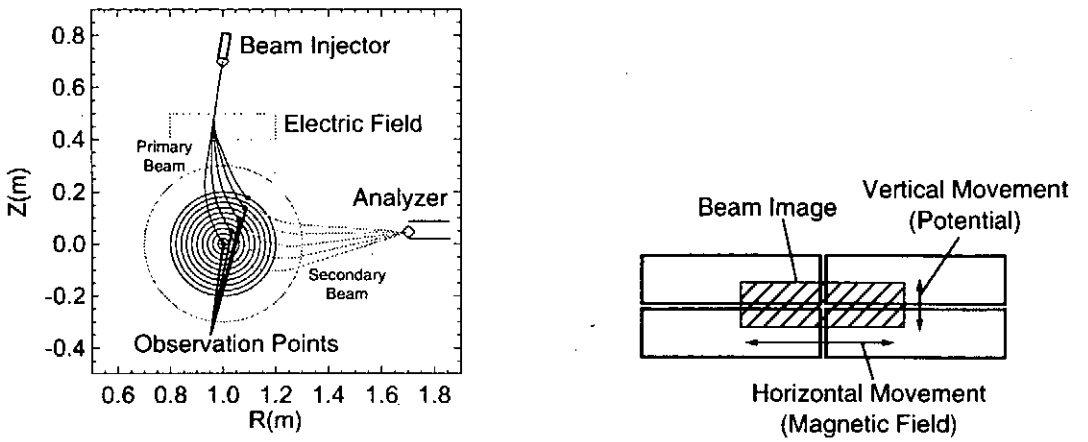

(a) (b)

Figure 1: (a) A schematic view of an HIBP system consisting of a beam injector, an energy analyzer and beam sweep plates, and assumed orbits in the calculation. The rectangular termed electric field means a region of a sweep plate to control the primary beam orbit and to change observation point. (b) A schematic view of a split plate detector set in the energy analyzer to detect the secondary beam.

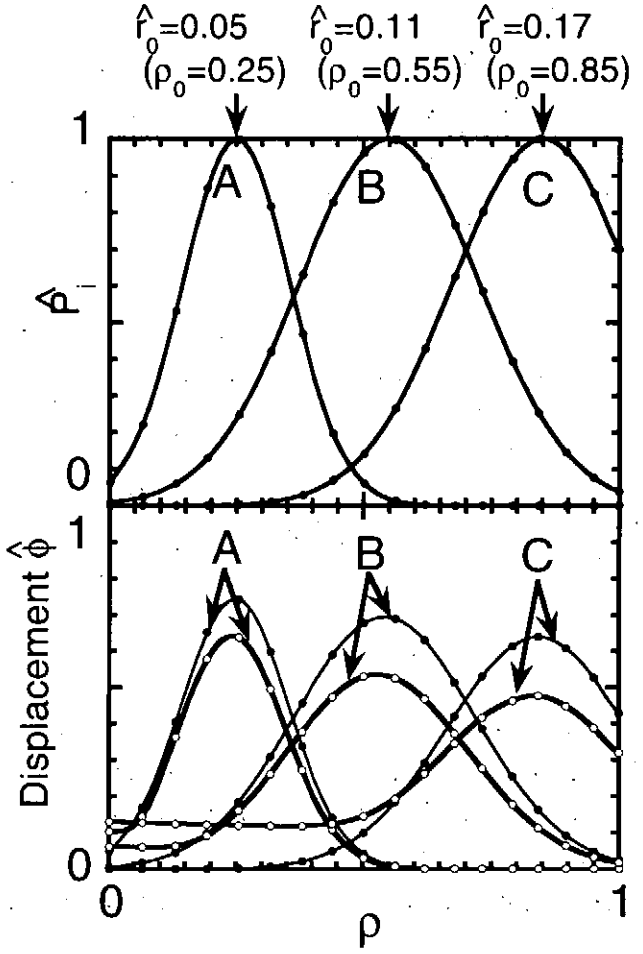

Figure 2: Upper: The profiles of normalized fluctuation amplitude, $\hat{P}_i = \exp\left(-\left(\hat{r}-\hat{r}_0\right)^2/\hat{r}_w^2\right)$. The $\hat{r}_0$ and ρ_0 mean the minor radius normalized by R_0 and the minor radius normalized by a, where the profile has maximum. The profiles of three cases in which $\hat{r}_0, r_w =$ (A) $0.05, 0.03$, (B) $0.11, 0.05$, (C) $0.17, 0.05$, are shown in this figure. Lower: The profiles of normalized beam angle displacement to toroidal direction, $\sqrt{\left\langle \hat{\phi}_D^2 \right\rangle}$ (thick solid lines) and the square root of local term A_1 in Eq. (7) (thin solid lines). The poloidal mode number $m = 2$, correlation length $\hat{\ell}_c = 0.1$, radial wave length $\hat{\lambda}_r = 0.1$ are assumed in the calculation.

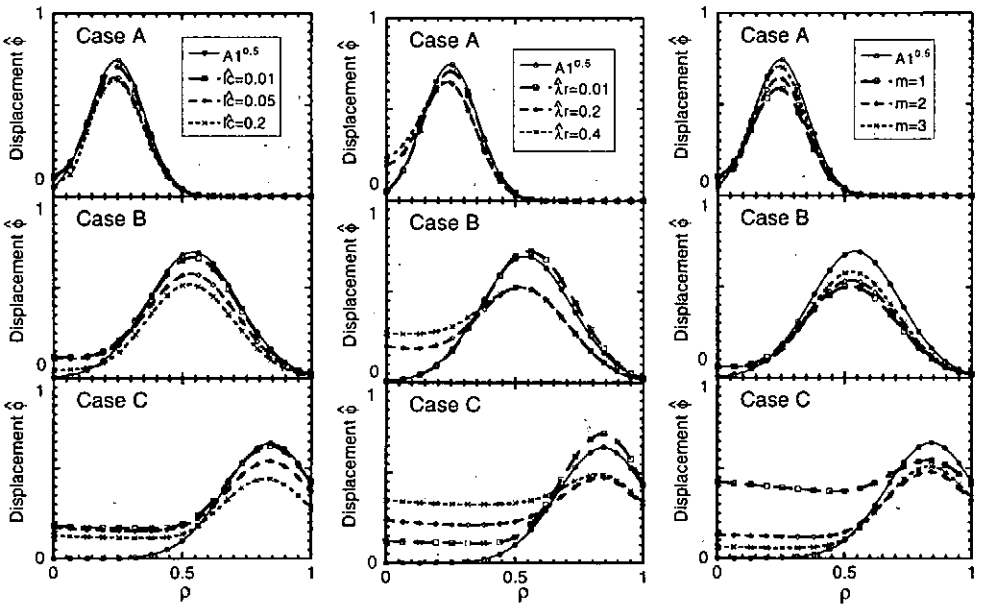

(a) (b) (c)

Figure 3: (a) The calculation result of $\hat{\ell}_c$ scan with m and $\hat{\lambda}_r$ being fixed to 2 and 0.1, respectively. $\sqrt{A_1}$ is shown as solid lines. Dashed lines are the square of normalized beam angle displacement, $\left\langle \hat{\phi}_D^2 \right\rangle$. (b) The calculation result of $\hat{\lambda}_r$ scan with m and $\hat{\ell}_c$ being fixed to 2 and 0.1, respectively. (c) The calculation result of m scan with $\hat{\ell}_c$, $\hat{\lambda}_r$ being fixed to 0.1, and 0.1, respectively. The poloidal mode number m is changed from 1 to 3.

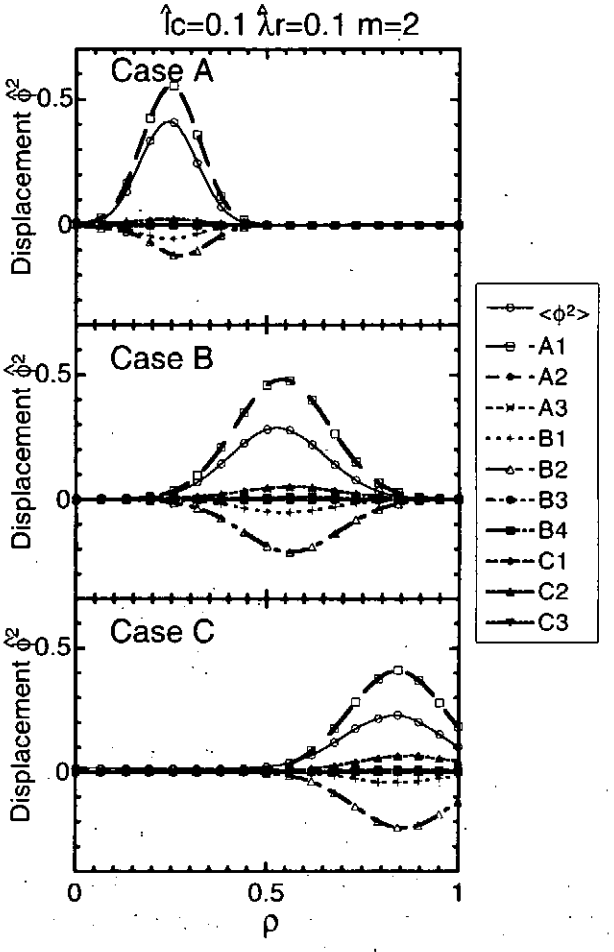

Figure 4: An example of individual contributions of path integral components, from B_1 to C_3, in the normalized angle displacement. The beam angle displacement $\left\langle \hat{\phi}_D^2 \right\rangle$ is shown as thin solid line. The largest contribution in path integral terms comes from B_2, which is the first order path integral term on secondary beam path.

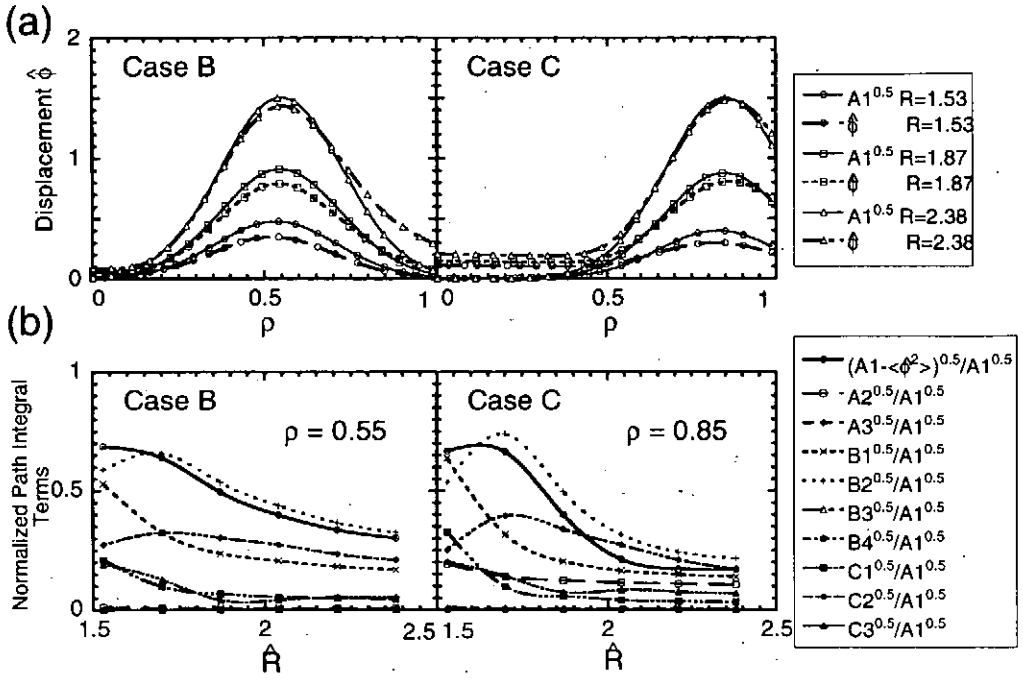

Figure 5: A trial to find an appropriate position of energy analyzer for the magnetic field fluctuation measurements with HIBP. (a) The dependence of beam angle displacement $\sqrt{\left\langle \hat{\phi}_D^2 \right\rangle}$ on the position of diagnostic point. Thin solid lines are profiles of the square root of local term A_1. (b) The ratio of path integral terms to the local term, A_1, as a function of major radius of diagnostics point. The difference between the beam angle displacement and the local term, $(A_1 - < \hat{\phi}^2 >)^{0.5}/A_1^{0.5}$, is shown as solid lines. The calculation is performed for case B and C. The presented values are those at $\rho = 0.55$ and at $\rho = 0.85$ for case B and C, respectively.

Recent Issues of NIFS Series

NIFS-772 M. Stepic, L. Hadzievski and M.M. Skoric
Modulation Instability in Two-dimensional Nonlinear Schrodinger Lattice Models with Dispersion and Long-range Interactions
Jan. 2003

NIFS-773 M.Yu. Isaev, K.Y. Watanabe, M. Yokoyama and K. Yamazaki
The Effect of Hexapole and Vertical Fields on α-particle Confinement in Heliotron Configurations
Mar. 2003

NIFS-774 K. Itoh, S.-I. Itoh, F. Spineanu, M.O. Vlad and M. Kawasaki
On Transition in Plasma Turbulence with Multiple Scale Lengths
May 2003

NIFS-775 M. Vlad, F. Spineanu, K. Itoh, S.-I. Itoh
Intermittent and Global Transitions in Plasma Turbulence
July 2003

NIFS-776 Y. Kondoh, M. Kondo, K. Shimoda, T. Takahashi and K. Osuga
Innovative Direct Energy Conversion Systems from Fusion Output Thermal Power to the Electrical One with the Use of Electronic Adiabatic Processes of Electron Fluid in Solid Conductors.
July 2003

NIFS-777 S.-I. Itoh, K. Itoh and M. Yagi
A Novel Turbulence Trigger for Neoclassical Tearing Modes in Tokamaks
July 2003

NIFS-778 T. Utsumi, J. Koga, T. Yabe, Y. Ogata, E. Matsunaga, T. Aoki and M. Sekine
Basis Set Approach in the Constrained Interpolation Profile Method
July 2003

NIFS-779 Oleg I. Tolstikhin and C. Namba
CTBC A Program to Solve the Collinear Three-Body Coulomb Problem: Bound States and Scattering Below the Three-Body Disintegration Threshold
Aug. 2003

NIFS-780 Contributions to 30th European Physical Society Conference on Controlled Fusion and Plasma Physics (St.Petersburg, Russia, 7-11 July 2003) from NIFS
Aug. 2003

NIFS-781 Ya. I. Kolesnichenko, K. Yamazaki, S. Yamamoto, V.V. Lutsenko, N. Nakajima, Y. Narushima, K. Toi, Yu. V. Yakovenko
Interplay of Energetic Ions and Alfvén Modes in Helical Plasmas
Aug. 2003

NIFS-782 S.-I. Itoh, K. Itoh and M. Yagi
Turbulence Trigger for Neoclassical Tearing Modes in Tokamaks
Sep. 2003

NIFS-783 F. Spineanu, M. Vlad, K. Itoh, H. Sanuki and S.-I. Itoh
Pole Dynamics for the Flierl-Petviashvili Equation and Zonal Flow
Sep. 2003

NIFS-784 R. Smirnov, Y. Tomita, T. Takizuka, A. Takayama, Yu. Chutov
Particle Simulation Study of Dust Particle Dynamics in Sheaths
Oct. 2003

NIFS-785 T.-H. Watanabe and H. Sugama
Kinetic Simulation of Steady States of Ion Temperature Gradient Driven Turbulence with Weak Collisionality
Nov. 2003

NIFS-786 K. Itoh, K. Hallatschek, S. Toda, H. Sanuki and S.-I. Itoh
Coherent Structure of Zonal Flow and Nonlinear Saturation
Dec. 2003

NIFS-787 S.I. Itoh, K. Itoh, M. Yagi and S. Toda
Statistical Theory for Transition and Long-time Sustainment of Improved Confinement State
Dec. 2003

NIFS-788 A. Yoshizawa, S.-I. Itoh, K. Itoh and N. Yokoi
Dynamos and MHD Theory of Turbulence Suppression
Dec. 2003

NIFS-789 V.D. Pustovitov
Pressure-induced Shift of the Plasma in a Helical System with Ideally Conducting Wall
Jan. 2004

NIFS-790 S. Koikari
Rooted Tree Analysis of Runge-Kutta Methods with Exact Treatment of Linear Terms
Jan. 2004

NIFS-791 T. Takahashi, K. Inoue, N. Iwasawa, T. Ishizuka and Y. Kondoh
Losses of Neutral Beam Injected Fast Ions Due to Adiabaticity Breaking Processes in a Field-Reversed Configuration
Feb. 2004

NIFS-792 T.-H. Watanabe and H. Sugama
Vlasov and Drift Kinetic Simulation Methods Based on the Symplectic Integrator
Feb. 2004

NIFS-793 H. Sugama and T.-H. Watanabe
Electromagnetic Microinstabilities in Helical Systems
Feb. 2004

NIFS-794 S.I. Kononenko, O.V.Kalantaryan, V.I. Muratov and C. Namba
Spectral and Angular Characteristics of Fast Proton-Induced Luminescence of Quartz
Mar. 2004

NIFS-795 K. Itoh, K. Hallatschek and S.-I. Itoh
Excitation of Geodesic Acoustic Mode in Toroidal Plasmas
Mar. 2004

NIFS-796 A. Shimizu, A. Fujisawa, S. Ohshima and H. Nakano
Consideration of Magnetic Field Fluctuation Measurements in a Torus Plasma with Heavy Ion Beam Probe
Mar. 2004